Journal of Marine Research, 52, 459–487, 1994

Dense overflow into a large silled embayment: Tidal modulation, fronts and basin modes

by M. White[1,2] and Alex E. Hay[1]

ABSTRACT

A dense bottom overflow into a 100-km scale silled embayment has been observed for a 70-day period using a coherent array of current meters and thermistor chains. As the internal Rossby radius is less than the width of the bay, the overflow is controlled by rotational dynamics. The flow is strongly modulated by the tide at diurnal, semi-diurnal and fortnightly periods. This causes a series of cold temperature fronts, associated with separate overflow events, to pass through the mooring array.

The overflow is also modulated at periods of 2–3 days. This appears to be associated with the interaction of the density current with bottom-trapped waves, or possibly with interior basin modes. It appears that the forcing of the oscillation is associated with the wind, which also contains a 3-d signal.

1. Introduction

Gravity currents play an important role in the dynamics of the deep ocean. The dense waters of the deep ocean are supplied from marginal seas adjacent to the main ocean basins. These source areas are relatively shallow, and the exchange of dense water occurs as a gravity current. In the Southern Ocean overflow occurs over large areas along the shelf break at the edge of the Weddell Sea. Other source regions in the Atlantic are separated from the deep ocean by a narrow channel with a shallow sill. In the North Atlantic the Mediterranean outflow through the Strait of Gibraltar is found at mid depth (Stanton, 1983; Zenk and Armi, 1990; and Price *et al.,* 1993). Bottom water outflow from the Norwegian and Greenland seas occurs through the Denmark Strait (Smith, 1976; Dickson *et al.,* 1990), and the Faeroe Bank Channel (Saunders, 1990). These deep flows are at a scale large enough that rotation affects the dynamics and the currents are controlled by a balance between gravity and Coriolis forces, bottom friction and mixing with the overlying fluid.

Mechanisms controlling the time-variability of these dense overflows are of fundamental interest. In deep ocean overflows, the available measurements indicate that on time scales less than a year, this variability is mainly confined to the high

1. Department of Physics, Memorial University of Newfoundland, St. John's, Newfoundland, Canada, A1B 3X7.

2. Present address. Department of Oceanography, University College, Galway, Ireland.

frequency end of the spectrum: that is, to time scales of a few days. For example, little seasonal variability has been observed in the Denmark Strait overflow (Dickson *et al.*, 1990), although fluctuations with a period of a few days were found (Dickson *et al.*, 1990; Smith, 1976). Smith (1976) has attributed the 2-d period variability to baroclinic instability in the Denmark Strait overflow. Saunders (1990) found fluctuations with period 3 and 6 days in the warm water flow through the Faeroe Bank Channel at a level above the cold dense bottom flow into the Atlantic. No evidence of seasonal variations in the outflow was found. Observations of the Mediterranean outflow have revealed that the low frequency variability with periods greater than 2 d can be due to meteorological forcing. For example, Stanton (1983) has related the largest fluctuations in the outflow to extremes in atmospheric pressure differences across the Strait of Gibraltar. Sharp changes in the temperature and thickness of the outflow have been attributed to the formation of shocks resulting from an increase in upstream transport (Nof, 1984).

Dense overflows can also accompany the renewal of deep water in semi-enclosed deep coastal basins and fjords, providing opportunity to study overflows at smaller scales. Often the width of the embayment is less than the Rossby radius and the overflow is then controlled by nonrotating dynamics. This is generally the case in narrow fjords (Gade and Edwards, 1980; Farmer and Freeland, 1983). Both the tide and wind-driven upwelling on the shelf generally provide the external forcing needed to bring water of sufficient density outside the sill up to a level above the sill depth to begin the exchange. Vertical mixing due to the tide may also control the timing of exchange for bays that have a sill of large horizontal extent relative to the tidal excursion (Geyer and Cannon, 1982).

This study is concerned with the summertime overflow of cold water from the Labrador Current on the Newfoundland Shelf into Fortune Bay. Fortune Bay is connected to the shelf via a narrow channel with a shallow sill, but the main basin is wide enough that rotation effects may be expected to play a role in the overflow dynamics. The situation is therefore analogous to that found in the ocean-scale overflows mentioned above. The paper describes the dynamics of the overflow, and in particular the variability of the flow and the coherency of the motions within the bay. Of particular interest are the possible interactions between the overflow and the internal modes of the basin. In anticipation of the results to be presented, consider a basin $O(100$ km) long, like Fortune Bay. The phase speed of long internal waves would normally be $O(1$ m/s), using typical values for Fortune bay of $g' = 0.002$ m s^{-2} and $h = 350$ m. The period of the gravest mode of such a basin would therefore be $O(2$ d): comparable to the period of the diurnal tide, and in the same range as the periods associated with weather systems. In such cases, therefore, some overlap would be expected between the spectrum of basin modes and the spectrum of the forcing.

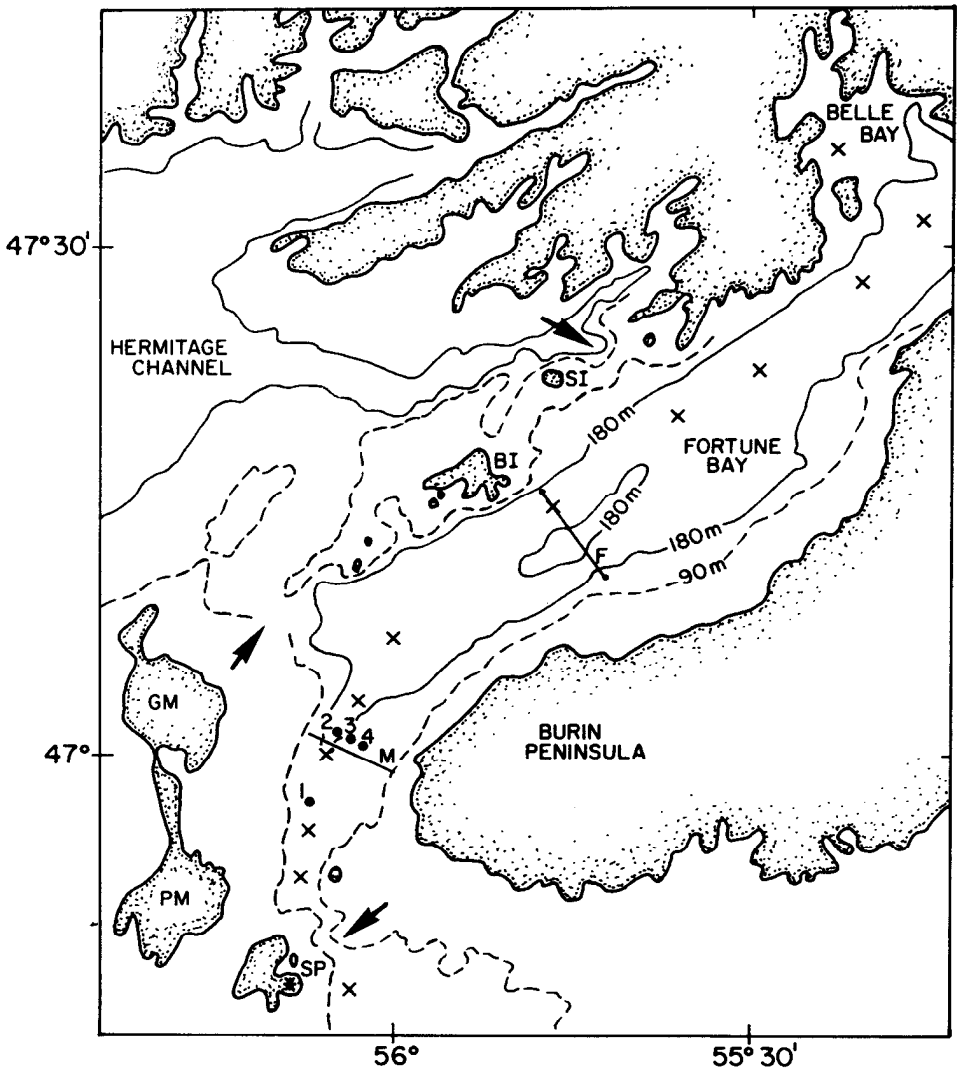

Figure 1. Fortune Bay showing the location of the mooring array and CTD stations. The numbered circles indicate mooring positions, the lines CTD sections across the bay, and x's the CTD stations along the axis of the bay. St. Pierre airport is indicated by the asterix and the lettered islands are; SP—St. Pierre, GM—Grande Miquelon, PM—Petite Miquelon, SI—Sagona Island and BI—Brunette Island. The arrows indicate the positions of the sills mentioned in the text.

2. Study area

Fortune Bay is located on the south coast of Newfoundland bounded by the Burin Peninsula and the Hermitage Channel (Fig. 1). It is approximately 120 km long and 5–20 km wide. The main basin has a maximum depth of 420 m, although the deepest

Table 1. Mooring locations.

Mooring	Lat	Long	Depth	Current Meter depths	Thermistor chain depth range
M1	46° 56.7	56° 08.6	159 m	112,154 m	118–148 m
M2	47° 01.6	56° 05.4	236 m	189,232 m	197–227 m
M3	47° 01.2	56° 04.6	183 m	134,177 m	failed
M4	47° 00.8	56° 03.2	146 m	101,144 m	109–139 m

point (526 m) is at the head of the bay. The bay has three outer sills: the Miquelon sill, north east of Miquelon Island (depth 115 m); the Sagona sill, east of Sagona Island (depth 110 m); and St. Pierre sill, between the Burin Peninsula and the island of St. Pierre (depth 125 m). The Miquelon and Sagona sills provide links to the Hermitage Channel, at the NW entrance to the bay. Previous observations of overflows from the surrounding channels into the bay have been documented by DeYoung and Hay (1987) and Hay and DeYoung (1989). These studies have shown that there is an annual winter overflow from the Hermitage Channel followed by a summertime overflow from the St. Pierre Channel. During the summer, the Labrador Water which overflows from the St. Pierre Channel gradually erodes the deep water remaining from the previous winter, until deep water replacement occurs.

Outside the St. Pierre sill at the SE entrance to the bay, the shelf is relatively deep due to the presence of the St. Pierre Channel, a continuation of the Avalon Channel separating Newfoundland and the Grand Banks. Cold water derived from the inshore branch of the Labrador Current is carried westward by this channel system. During summer, this cold water is observed to flow over the St. Pierre sill into Fortune Bay as a dense bottom current (DeYoung and Hay, 1987; Hay and DeYoung, 1989).

The closed 180-m contour in the main Fortune Bay basin represents a central plateau. This feature is of some importance to the later discussion.

3. Measurements

Measurements were made using an array of 4 current meter/thermistor chain moorings for a period of 70 days, between late June (Julian Day (JD) 180)–early September (JD 250) 1984, together with a series of CTD transects along and across the bay (Fig. 1). Table 1 summarizes the location/depths and instrumentation of each mooring. Each mooring consisted of two Aanderaa current meters (CM) located 5 m and 50 m above the seabed, together with a thermistor chain, having 11 sensors 3 m apart, located between the current meters. One mooring was positioned just inside the inner St. Pierre sill and the other 3 were located in a line across the bay approximately 10 km from the sill mooring. The actual distances ranged from 10 to 10.4 km, depending on the mooring. The thermistor chain on mooring M3 failed and the data from the upper current meter on that mooring is also unsuitable for analysis

due to a problem with the current meter vane. The axis of the main bay is approximately directed SW–NE, but in the region of the mooring array, the along-bay direction is taken to be 27°True. In this paper, the horizontal velocities will be denoted (u, v) directed in the across-bay (or x, 117°True) and along-bay (or y, 27°True) directions.

CTD transects were also made both along and across the bay during the deployment and recovery cruises. These include an along-bay transect, ranging from outside the St. Pierre sill to Belle Bay (Fig. 1), and several across-bay transects. In addition wind measurements, recorded at the airport on St. Pierre, were also available.

4. Observations

a. Density structure. Figure 2 shows temperature and density sections along the axis of the bay, the σ_t values calculated from CTD measurements. The section is along the deepest part of the bay, as indicated in Figure 1. The dashed line represents the central plateau in the main basin. A temperature minimum is present within the bay centered at about 120 m depth. The increased temperatures below this depth are a result of the overflow of warm, saline water from Hermitage Channel the previous winter (Hay and DeYoung, 1989).

Cold and relatively dense water is present above the level of the sill, marked by a temperature front. Some of the cold water can be seen to have spilled into the bay a distance of 10–20 km from the inner sill (located at a distance of 25 km on the axis of the transect). This cold water is not observed in the along-bay section at a point beyond the start of the plateau region. This is because at this time the cold inflow passed the plateau on the SE side and not in the deeper channel where the CTD transect was made, as shown by the transverse temperature/density sections across the plateau (Fig. 3). Colder water, about 0.4°C, is seen on the right hand (SE) side. Figure 3 also shows evidence of circulation both round the base and top of the plateau. A transverse section close to the mooring line is shown in Figure 4. The core of the cold current is located on the east side of the channel and upslope of the deepest point. The density contours are tilted upward to the right, indicating that the Coriolis force is playing a role in the dynamics. These sections were made within a 1–2 h time period, and so are not tidally aliased.

Figure 5 shows the main features of the inflow. Contours of temperature interpolated from the thermistor chain and current meter data are shown with 3 hr mean currents superimposed. The sections run along the bay between M1–M2 and M1–M4 and across the bay at the mooring line M2–M4. Similar interpolated temperature fields were in good agreement with CTD sections made close to the mooring line at the same time. The two sections along the bay show a relatively strong bottom flow of cold water, both at the sill and at the mooring line, with little cross-bay velocity observed. High current shear was observed between the bottom flow and the

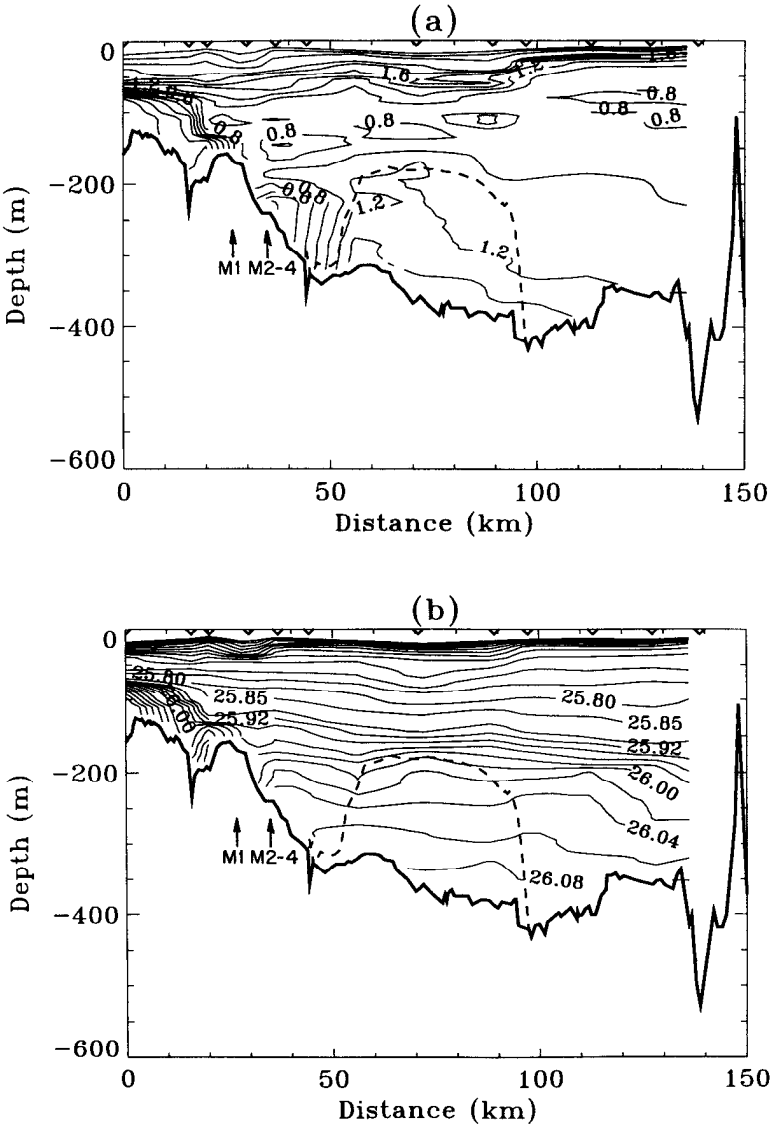

Figure 2. Along bay transect of (a) temperature and (b) σ_t made from the CTD stations indicated in Figure 1. The dashed line shows the location of the central plateau within the bay (shown in Figure 1 by the 180 m contour). Arrows indicate the positions of the sill mooring (M1) and the mooring line (M2-M4), and triangles the CTD stations. The contour intervals are 0.2°C below 2°C, and 1°C above 2°C for temperature, and 0.05 below 25.9 and 0.02 above 25.9 for σ_t.

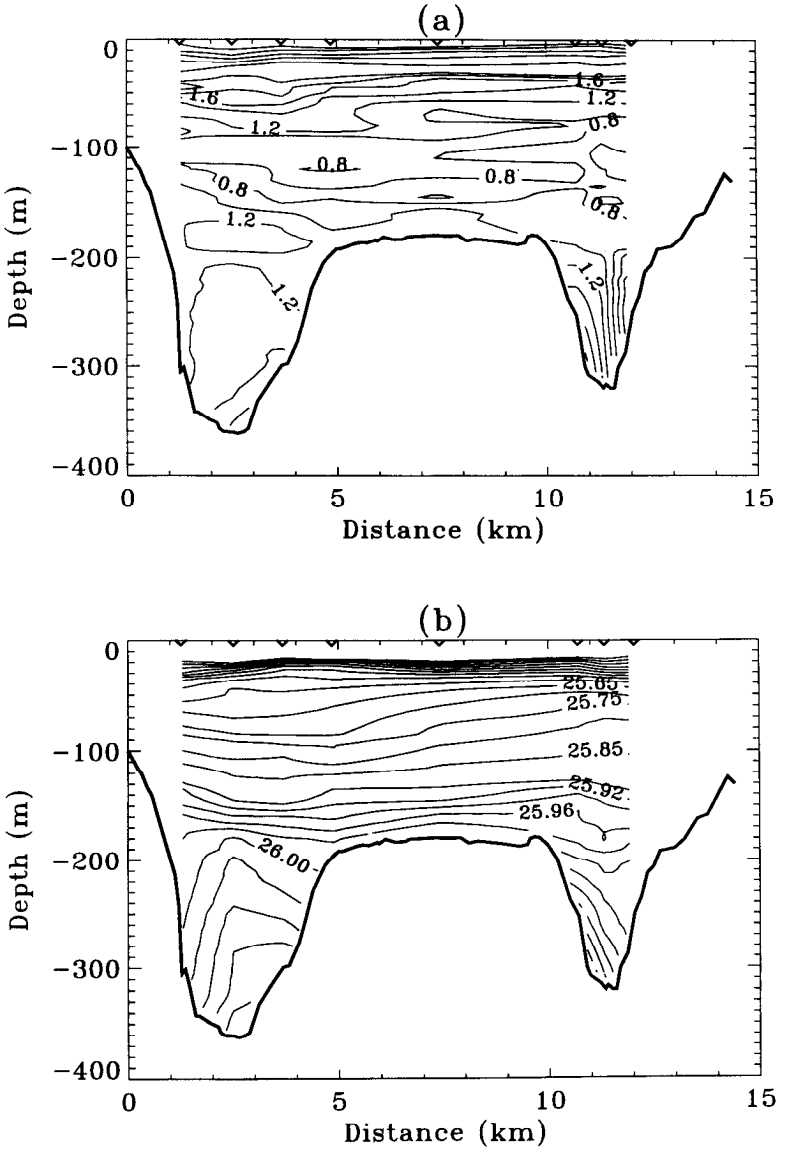

Figure 3. Across bay transect of (a) temperature and (b) σ_t across the plateau region marked by the line F in Figure 1. CTD stations are indicated by the triangles. The contour intervals are 0.2°C up to 2°C, and 1°C above 2°C for temperature and 0.05 up to 25.9 and 0.02 above 25.9 for σ_t. The transect is orientated such that into the page is directed into the bay.

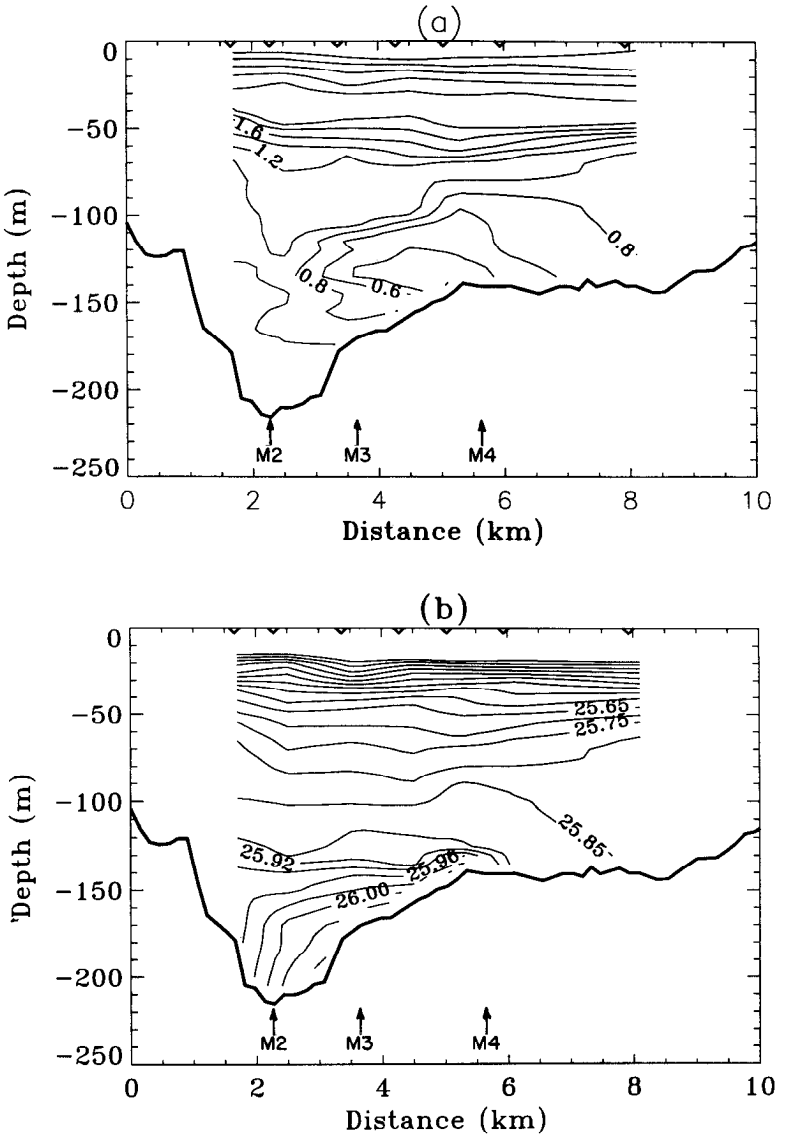

Figure 4. Across bay transect of (a) temperature and (b) σ_t close to the mooring line M2-M4. CTD stations are indicated by the triangles, and the mooring locations by arrows. The contour intervals are as for Figure 3.

overlying fluid. Note the reversal in the current direction measured by the upper current meter on mooring M2, located in the deepest part of the channel.

b. Velocity and temperature time series. Table 2 summarizes the mean currents and temperatures found for the 70 d observation period. Figure 6 shows the high pass

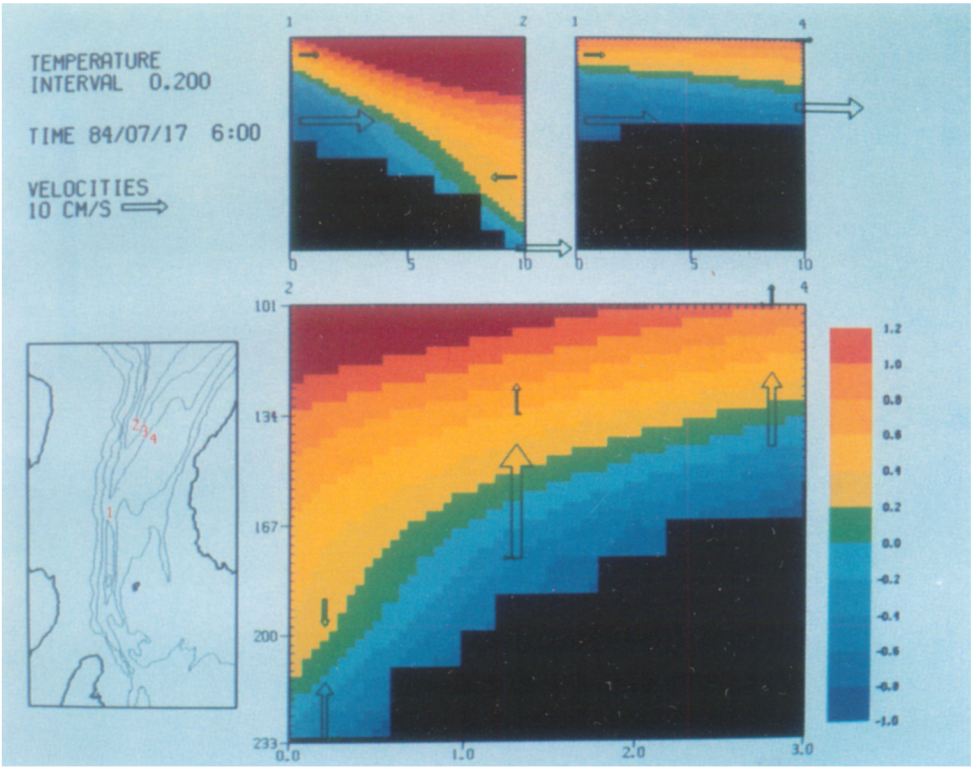

Figure 5. False color representation of temperature contours, with measured velocities superposed. Upper left: temperature and along-bay current, between M1-M2. Upper right: temperature and along-bay current, between M1-M4. Main panel: temperature and both along- and cross-bay currents, M2-M4. The upward pointing vectors indicate current into the bay. The contour interval is 0.2°C. The horizontal scale is distance in km, the vertical scale is depth in m. Both the width and length of the vectors scale linearly with velocity.

Table 2. Mean currents.

Mooring	Level	along-bay (v) cm s^{-1}	across-bay (u) cm s^{-1}	Temperature °C
M1	U	3.06	0.04	0.686
	L	14.7	−5.5	−0.638
M2	U	−1.3	−0.8	0.766
	L	12.4	2.6	−0.210
M3	U	fail	fail	0.656
	L	17.6	−3.0	−0.106
M4	U	0.5	1.3	0.803
	L	13.2	−0.9	0.010

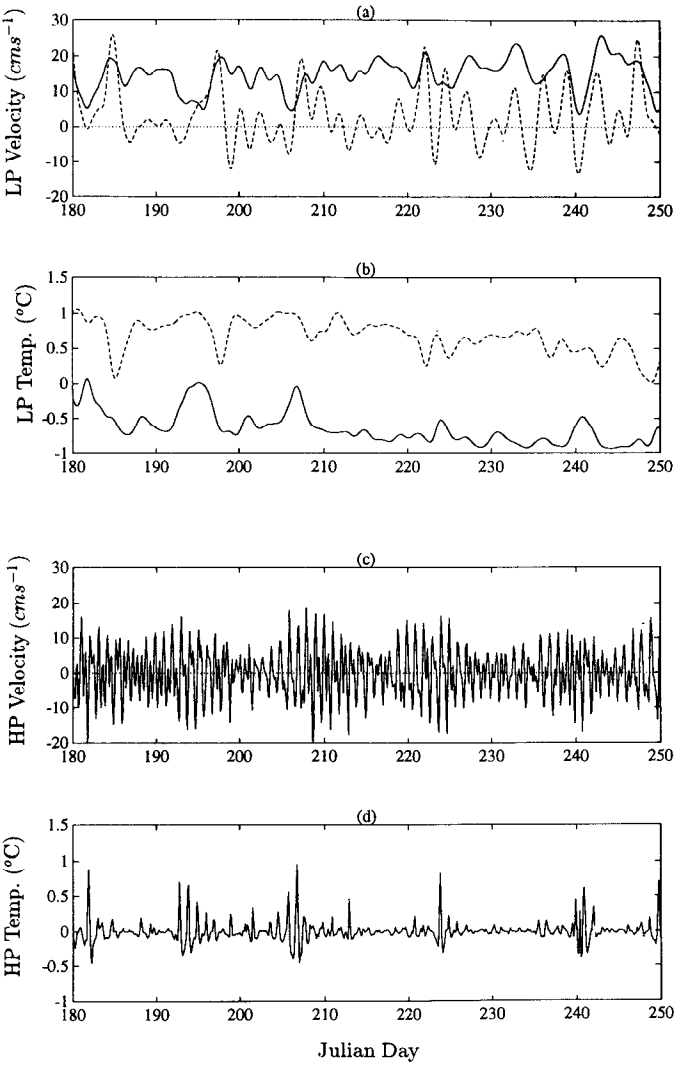

Figure 6. Time series of low pass filtered (LP, freq < 0.5 cpd) (a) along-bay current at lower (—) and (---) upper current meter, (b) temperature for the same current meters at the sill, and high-passed (HP) (c) along-bay current and (d) temperature for the lower current meter at the sill.

(HP) and low pass (LP) filtered time series of along-bay current and temperature for the current meters at the sill mooring (M1). The low-pass filter used was a 3rd order Butterworth filter with a cut-off frequency of 0.5 cpd. The high pass time series are defined as the difference between the original and filtered data. A continuous low frequency current into the bay was registered by the near bottom current meter with a mean of 15 cm s^{-1} (Fig. 6a). Lower temperatures are associated with higher rates of

inflow, indicating advection of colder water into the bay. During the 70-d measurement period, the temperature at both current meters steadily decreased (Figure 6b). At the upper level, there was no continuous low frequency flow into the bay, and several reversals in current direction were observed. Large inflow events, corresponding to low temperatures and high flow rates into the bay, were observed early in the record on days 185, 197 and 208. Initially, these events were registered by both upper and lower current meters. At the upper level, however, the initial peak in current and decrease in temperature were short-lived, compared to the O(5–7 d) duration of elevated currents and reduced temperatures at the lower current meter. The high frequency along-bay current/temperature time series show tidal variability at both the semi-diurnal and diurnal periods, as well as a strong spring-neap modulation (Fig. 6c,d).

Time series of low frequency current and temperature, for current meters on the mooring line M2-M4, are shown in Figure 7. Features similar to those observed at the sill mooring are apparent. Generally there was a mean inflow of O(15 cm s^{-1}) into the bay close to the seabed, with maximum flow at M3 (17 cm s^{-1}), the central mooring in the line, located part way up the slope (Fig. 5). The mean currents registered at the upper current meters were small.

A distinct oscillation, with a period of 2.5–3 d, is present in the measured currents. The oscillation is particularly apparent after Julian day 200. This oscillation took the form of an initial peak followed by an apparent decay in the oscillation amplitude. The oscillation was also present at all moorings and levels, but was more pronounced at the mooring line and at the upper current meter on the sill. At the mooring line, the oscillation can be seen both in the velocity and the temperature.

c. Density currents and fronts. The unsmoothed temperature measurements from the thermistor chains (20-min sampling interval) and current meters (15-min interval) revealed the passage of temperature fronts through the mooring array. Composite temperature time series are shown in Figure 8 for one 6-d period. The unaveraged (15-min) currents at the lower current meters are also shown.

Figure 8 illustrates a series of fronts during a period immediately preceding peak spring tides (see Fig. 6c). Focussing attention first on Figure 8b (mooring M2), there were several times when the temperature dropped by 0.5°C or more at all the thermistors on the mooring. These times were separated by about one day (diurnal frequency). The marked reduction in temperature indicated the passage of a cold front. The changes in temperature at M4 (Fig. 8a) were generally of a lesser magnitude and often the upper sensors in the vertical array showed little or no temperature decrease. The fronts were also observed at the sill mooring (Fig. 8c). The passage of each individual front was observed in sequence: first at the sill (M1), then at M2 and later still at M4. The time delay between occurrence of the cold fronts at M1 and the mooring line (M2 and M4) varied between 4 and 8 hours. This

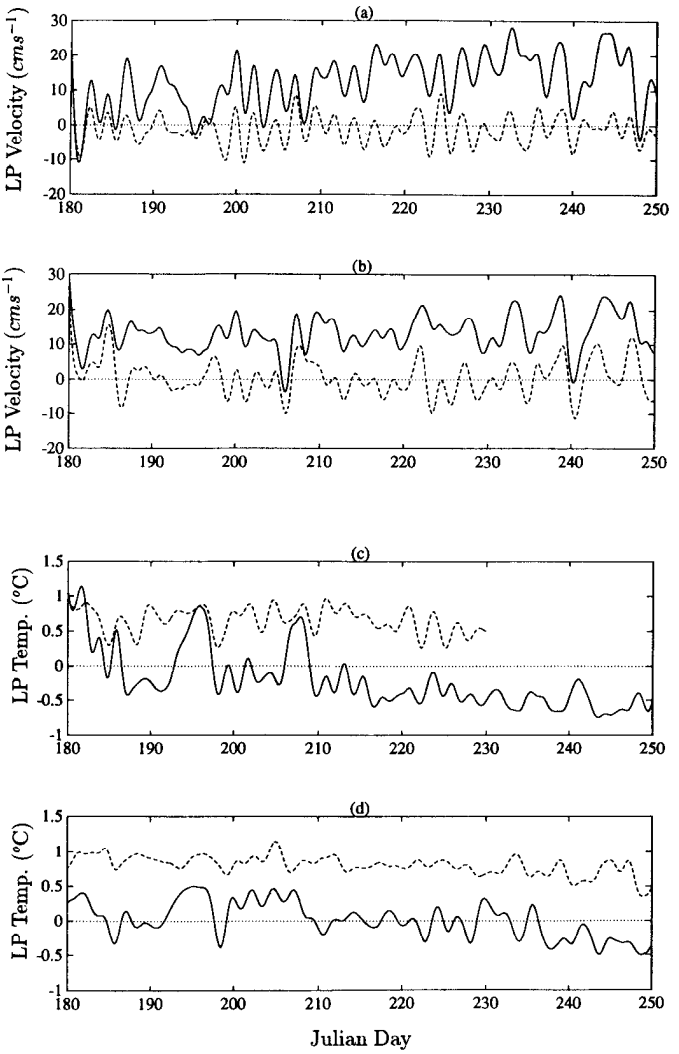

Figure 7. Low pass filtered (LP, freq < 0.5 cpd) time series of along-bay current at (a) M2, (b) M4, and temperature at (c) M2 and (d) M4. Lower current meter records are shown (—) and upper current meters (---).

yields propagation velocities of 35–70 cm s^{-1}. At any given mooring, the decrease in temperature occurred first at the lowest sensor and progressively later at the upper sensors. A time delay of O(0.5–3 h) was found between the temperature reduction at the lowest and uppermost sensors. After the passage of the front, the subsequent increase in temperature occurred first at the uppermost thermistor.

Figure 8d shows the unsmoothed along-bay current at the lower current meter for moorings M1, M2 and M4. The current was directed into the bay for most of this

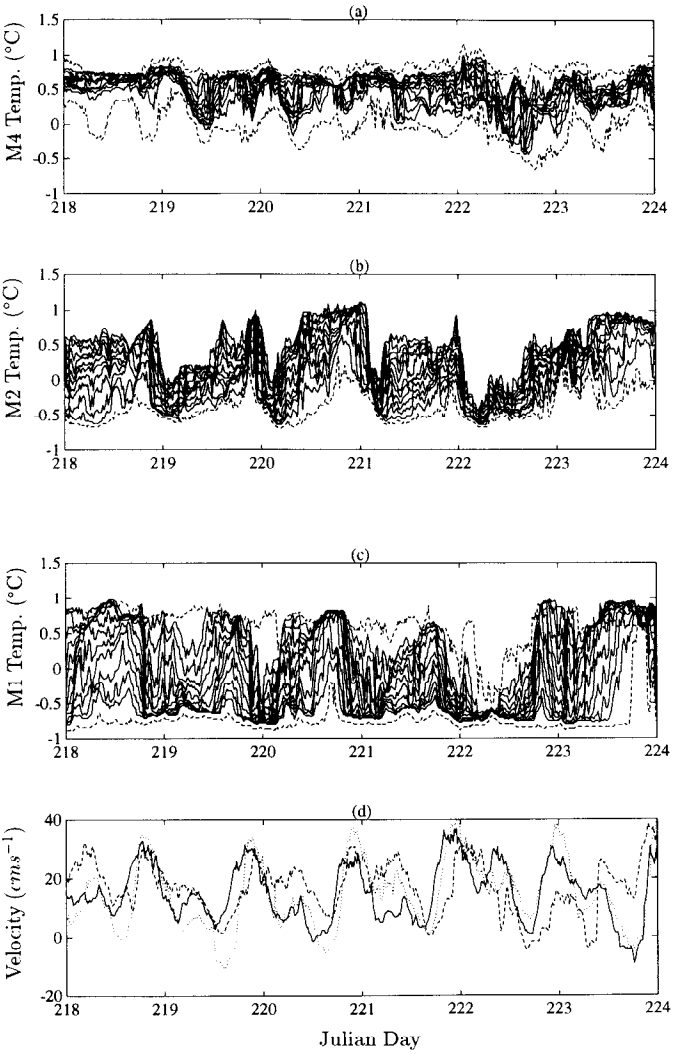

Figure 8. Six day time series, approaching spring tide, of temperature from moorings (a) M4, (b) M2 and (c) M1, derived from (—) thermistor chain and (---) current meter records. The currents for the same period are shown in (d) for the lower current meter on mooring (—) M1, (---) M2 and (····)

period with few reversals in current direction observed. Variability was mainly diurnal, with a smaller semi-diurnal period signal present. Peak currents were between 25–35 cm s^{-1} at all moorings. Decreases in temperature measured by each thermistor chain followed abrupt increases in the local inflow speed. This is especially apparent at the sill and at M2. These increases occurred first at M1 and up to

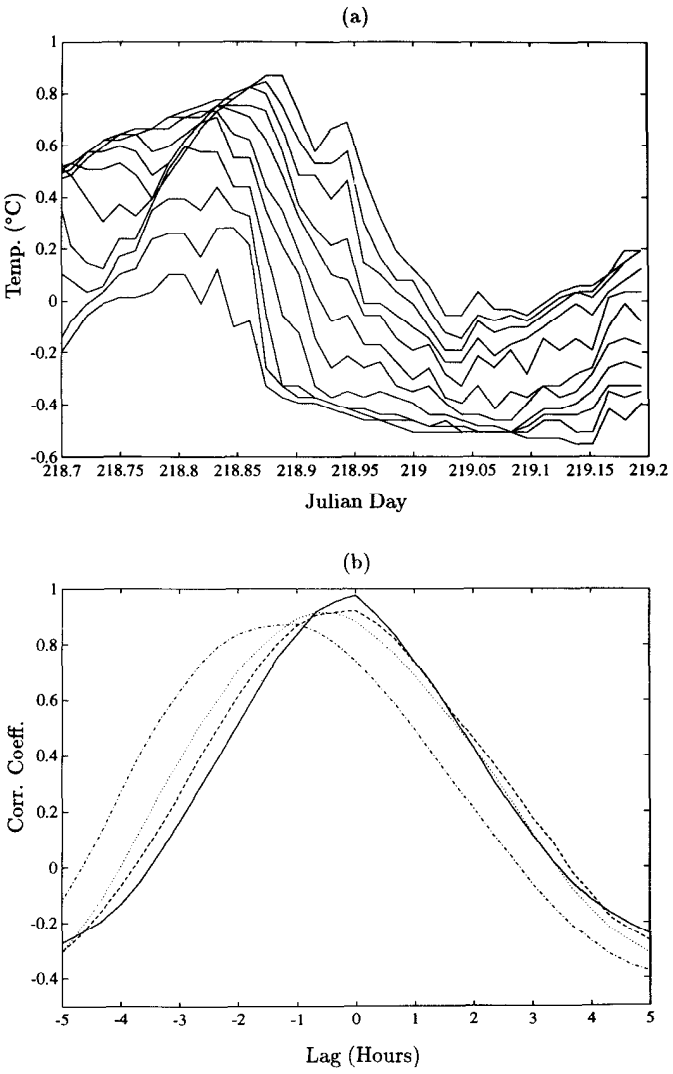

Figure 9. (a) 12 h time series of temperatures measured by the thermistor chain on M2 indicating the passage of the cold front shown in Figure 8b at day 219. The cross correlations between the temperature at the lowest thermistor in the array and those (—) 3 m, (---) 12 m, (····) 21 m and (-·-·) 30 m above that sensor are shown in (b). A negative lag indicates upper sensor lags the lower sensor.

4 h later at M4 and finally M2. Higher peak currents were found at M4 relative to M2. Note that this differs from the temperature results for these two moorings.

Figure 9 shows the temperature time series recorded by the thermistor chain at M2 for a 12-h period during the passage of one of the cold fronts shown in Figure 8. The temperature drops by up to 0.5° at all sensors. At the upper sensors in the array, this

temperature decrease noticeably lags that at the lower sensors. Figure 9b shows cross correlations between the temperature at the lowest sensor and 4 others located at progressively higher levels throughout the array. Generally there is an increasing phase lag and a reduction in the correlation coefficient with height above the lowest sensor. No measureable lag (recall that the sampling period was 20 min) occurred between the changes at the lowest sensor and those 3 m and 12 m above it. Peak correlations are observed at lags of 40 min and 60 min respectively for the sensors located 21 m and 30 m above the lowest sensor.

d. Winds. Figure 10 shows time series of the wind velocity recorded at St. Pierre airport (Fig. 1). The northeast component is approximately parallel to the axis of the main basin. The mean wind for the 70-d measurement period was 2.7 m s^{-1} directed toward 43°True, essentially parallel with the bay axis. Both the NE and SE components showed variability at long periods of O(10–15 d), as well as a fairly strong oscillation with a period of about 3 d. (Note that this period is similar to that observed in the current observations.) Power spectra (not shown) of these two components show the highest energy in the 2–10 day band, as expected in this region. In particular the SE component has significant peaks at the 3-d and 6-d periods.

Time-lagged correlation functions between the low frequency winds and the along-bay current registered by the upper meter at the sill are shown in Figure 10c. Generally the correlations are low. For the SE wind component, maximum correlation of only 0.4 was found with at a lag of −1.1 d. The NE wind and along-bay current were negatively correlated, with a peak negative correlation of about −0.3 at a lag of about −0.8 d. Both of these correlation peaks point to increased inflow being weakly correlated with wind blowing out of the bay. (The geometry of the SE entrance to Fortune Bay (Fig. 1) is complicated. There are two main entrance channels. In the vicinity of the sill mooring, winds blowing toward both the SE and the SW would be directed "out of the bay.")

e. Velocity spectra, and phase propagation. Figure 11 shows rotary spectra for all current meters on moorings M1, M2 and M4. The time series were split into two non-overlapping records of 32-d duration. The confidence limits are based on a minimum of 4 degrees of freedom, the number of degrees of freedom increasing with increasing frequency due to band-averaging. For all frequencies the two rotary components of current are generally of the same order of magnitude, although the clockwise component is the slightly larger of the two. This indicates that the flow was essentially uni-directional, consistent with the observation that the along-bay component dominated the mean current (Table 2). There are well defined peaks at the semi-diurnal and diurnal periods for all current meters. The inertial peak in the clockwise component is not significant except at the upper CM on M4, the shallowest of the current meters.

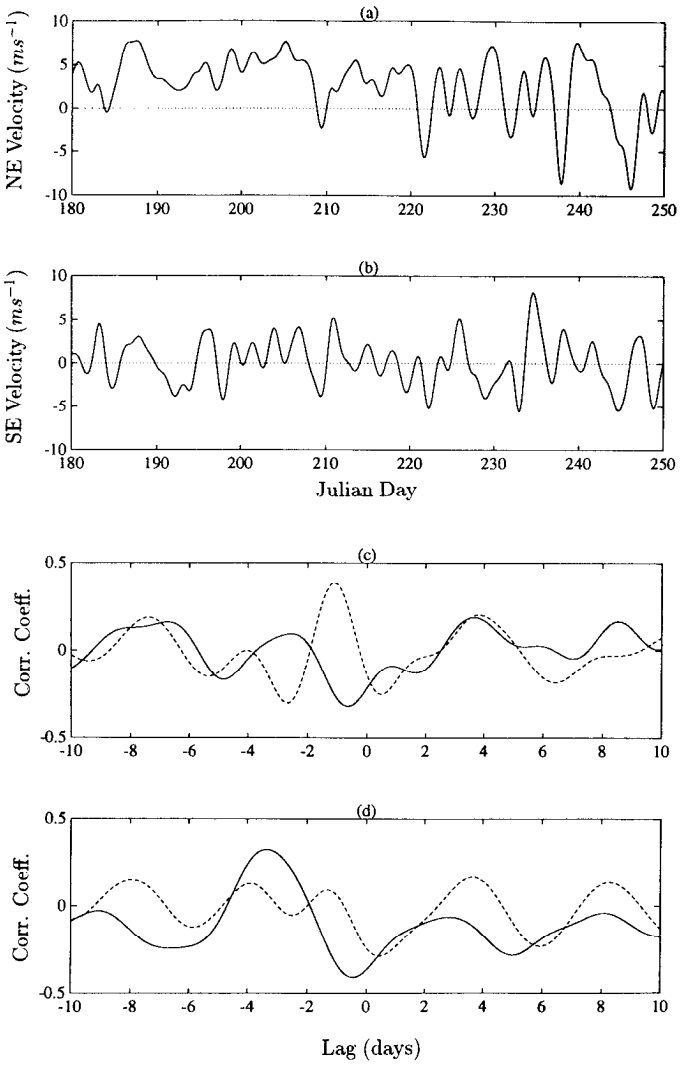

Figure 10. Time series of (a) NE and (b) SE wind components at St. Pierre airport, and time lagged correlation coefficients between the wind components and (c) upper and (d) lower current meter on M1. NE wind correlations are shown (—) and SE correlations (---). A negative time lag indicates current lagging the wind.

A peak is present in the 0.3–0.6 cpd frequency band in all spectra. The peak has a smaller frequency bandwidth at the sill mooring and generally at the upper current meters relative to the lower. Among the upper current meters, the peak is largest at the sill mooring. At the lower current meters, this broad peak is amplified at the mooring line current meters (M2 and M4) relative to the sill current meter. There is also a broadening of the peak from the sill mooring to the mooring line current

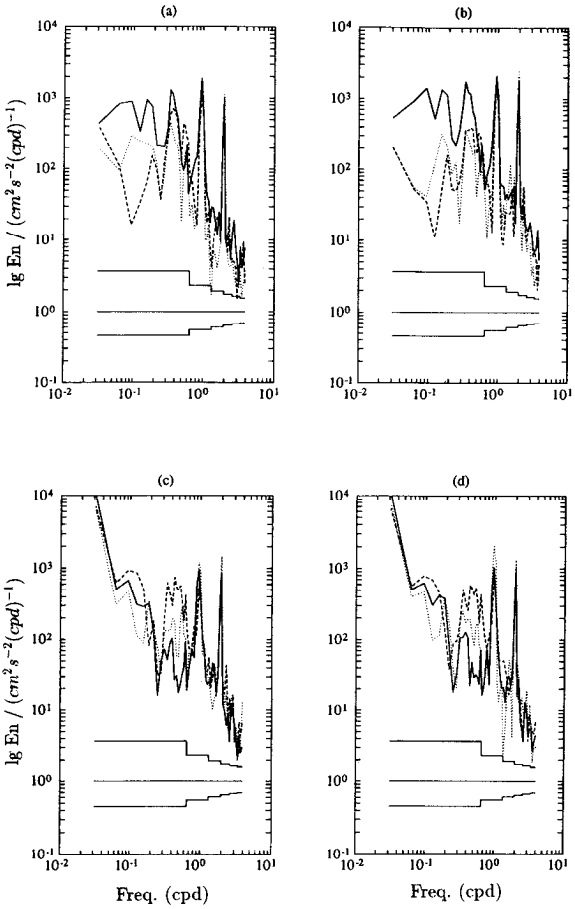

Figure 11. Rotary spectra for moorings (—) M1, (---) M2 and (····) M4, showing upper current meter (a) clockwise and (b) anticlockwise components. The corresponding components for the lower level current meters are shown in c and d. The 95% confidence limits are shown by the stepped line.

meters. An associated shift of the center of the peak to higher frequencies from the sill to the mooring line is also apparent. This is more clearly seen in the variance preserving power spectra of the lower along-bay currents, shown in Figure 12. These spectra show that the peak has highest amplitude at mooring M2. The peak is at least an order of magnitude greater at M2 than at the sill. The peak at M3 is also significantly larger than at the sill, with the increase in frequency bandwidth also apparent. The bandwidth at the sill is between 0.3–0.4 cpd (2.5–3.3 d) while at the mooring line the bandwidth has increased to between 0.3–0.6 cpd (1.3–3.3 d).

Analysis of the cross spectral coherency and time lagged correlations indicates a high degree of coherency in the motions between the moorings. Figure 13 shows an

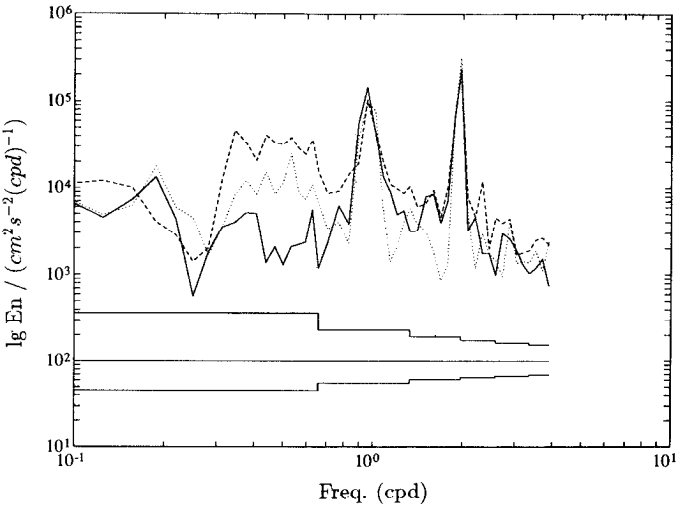

Figure 12. Variance perserving power spectra of along-stream velocity at the lower current meters on moorings (—) M1, (---) M2 and (····) M3. The 95% confidence limits are shown by the stepped line.

example: the coherency in the along-bay current between the upper and lower current meter pairs on moorings M1 and M2. The signals are highly coherent at the principal tidal periods and the 2.6-d oscillation period. This lends credence to the phase measurements made from the cross spectra, which are discussed below.

At the semi-diurnal period there is little phase difference in the along-bay current between the current meter pair on each mooring ($<10°$), suggesting that this component is dominated by the barotropic tide. There is high variability in the phase estimates for the across-bay current and temperature components, but for these time series the coherence is smaller. At the diurnal period, both current components at M1 (sill) and M2 show a mean phase difference of $O(35°)$ between each current meter pair, but with a different sign. Assuming a baroclinic wave motion there is upward phase propagation at the sill (i.e. downward energy propagation (Gill, 1982)) and downward phase propagation at M2. These inferred propagation directions are also found in temperature but the estimated phase difference is higher (60°). For the 45-m vertical separation between current meters, these phase differences imply a vertical wavelength of 270–450 m. These wavelengths are 2–3 times the water depth at M1 (Table 1).

There is an obvious visual correlation among the 2–3 day period oscillations present in the low-passed currents at all moorings shown in Figures 6 and 7. Figure 13 confirms this relatively high coherency in the 0.3–0.5 cpd band, for mooring M1 and M2, with a smaller coherence at lower levels (Fig. 13b). Generally the motion centered at the 2.6-d period is coherent between all the moorings, although the error bounds are large due to the short length of the time series. In particular the

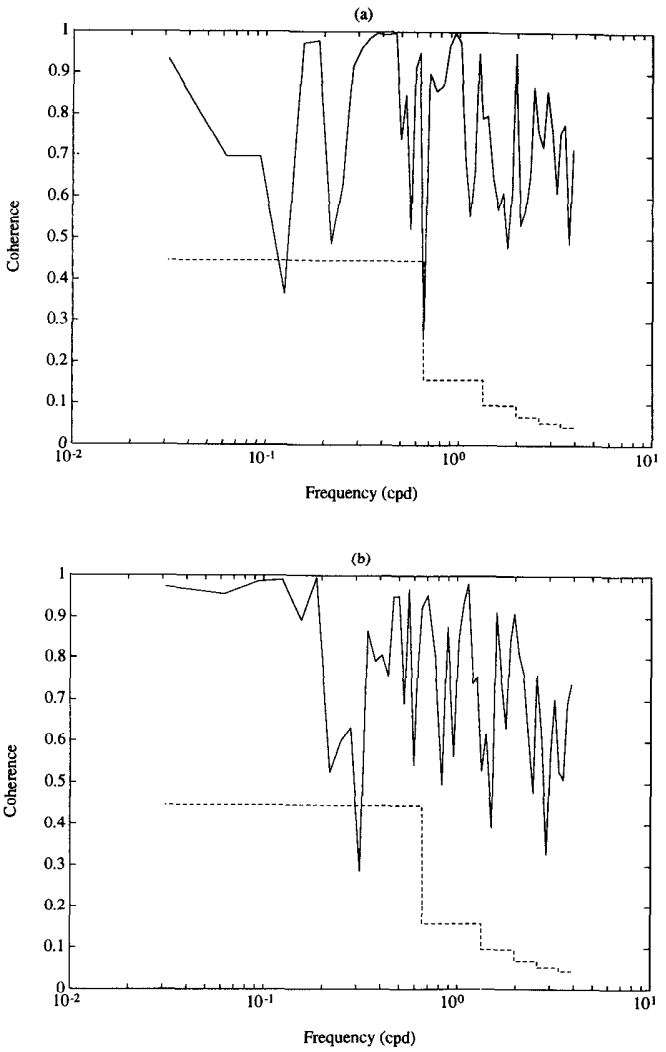

Figure 13. Coherence vs frequency for the (a) upper and (b) lower current meter pairs for the sill (M1) and M2 moorings. The 95% confidence limits are shown by the stepped line.

motion is coherent over the range of frequencies of the broad spectral peak at the upper current meter level.

The phase differences at the 2.6-d period obtained from the cross spectra for the lower current meters are shown in Figure 14. The phase difference between the lower level along-bay velocity at the sill and at moorings M3 and M4 are 23° and 28° respectively, with the sill current leading in both cases. This represents a phase velocity of 55–70 cm s^{-1} for a 2.6-d period wave. If the upper CM at the sill is used

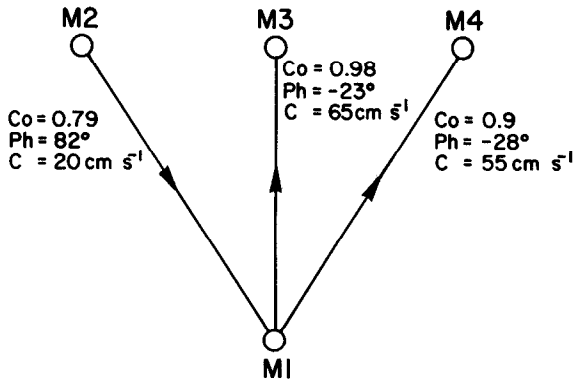

Figure 14. Phase propagation at the 2.6 day period, together with coherence values and inferred phase velocities, between lower current meter pairs. Arrows indicate direction of propagation.

instead of the lower CM, similar phase differences are observed. Between moorings M2 and M1 there is a phase difference of 82°, with phase propagating toward the sill. This indicates a phase velocity of about -20 cm s^{-1}. The along-bay velocity at the lower level current meters is also coherent along the mooring line, with a phase difference of 104° between M2–M3 and a much smaller difference (11°) between M3–M4, with phase propagating from M2 to M4. For the temperature spectra, the phase differences and coherency are much less well defined, and are not significant at the 95% level.

f. Vertical shear. Phase measurements from the power spectra suggest that a baroclinic motion is present at the diurnal frequency at M1 and M2. Figure 15 shows the spectra of velocity shear at the moorings M1, M2 and M4. The velocity shear was estimated from the 45-m vertical separation between the 2 current meters. A peak in the shear spectrum at the diurnal period is present for moorings 1 and 2, which is an order of magnitude smaller at M4. For all 3 moorings the peak at the semi-diurnal period is relatively small compared to the diurnal peak, indicating that the semidiurnal tide is mainly barotropic. A relatively large peak at approximately the 2.6-d period of only 0.38 is observed for the sill mooring, which is less apparent at M2 and M4.

5. Discussion

a. Mean currents and fronts. The internal deformation radius for the overflow is given by

$$a = (g'h)^{1/2}/f, \tag{1}$$

where g' is the reduced gravity and h the overflow thickness. For the St. Pierre sill,

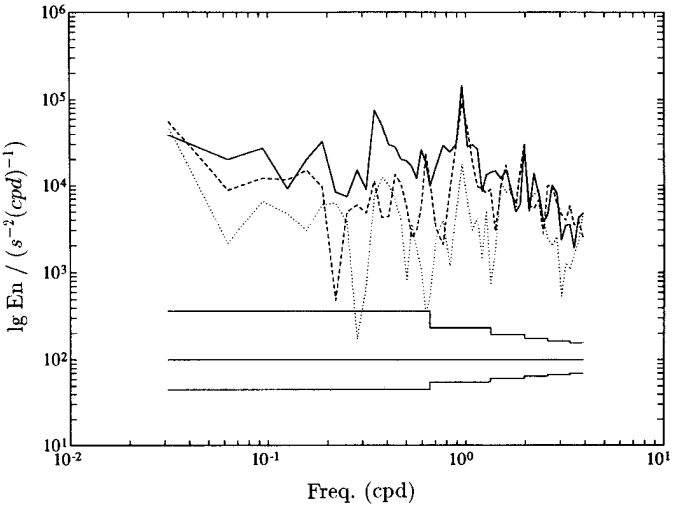

Figure 15. Power spectra of current shear at moorings (—) M1, (---) M2 and (····) M4. The 95% confidence limits are shown by the stepped line.

the mean height of the overflow was taken to be 25 m, the mean height above the seabed of the 0°C isotherm. $\Delta\rho/\rho$ for the overflow is about 2×10^{-4}, so that $g' = 0.002$ m s^{-2}. The internal Rossby radius will then be $a = 2$ km at the sill, less than the width of the bay. We may expect, therefore, that rotation will affect the dynamics of the overflow, similar to that observed in larger scale overflows (Smith, 1976; Dickson *et al.*, 1990; Saunders, 1990).

Assuming that the cross-stream momentum balance is approximately geostrophic gives

$$fV = g'\gamma_x \tag{2}$$

where V is the mean flow speed, f is the Coriolis parameter, and γ_x is the across-stream isopycnal slope. Values for γ_x are in the range 0.01–0.02 (Fig. 4). With $g' = 0.002$ m s^{-2}, this gives values of V in the 15–30 cm s^{-1} range. This is typical of the measured speeds.

The CTD sections show that the core of the cold water overflow is perched on the eastern slope of Fortune Bay above the deep channel. The maximum mean along-bay velocity was also recorded at M3 (lower), located at the center of the mooring line on the slope of the deep channel. This character is analogous to that observed in the Mediterranean outflow (Zenk and Armi, 1990), where the density flow occurred at mid-depth, perched against the continental slope. The behavior is included in Smith's (1975) streamtube model, in which the cross-stream momentum balance (integrated across the flow) is between the Coriolis acceleration and the cross-stream component of buoyancy parallel to the slope, with an additional centrifugal accelera-

tion due to the curvature of the streamtube axis. The centrifugal term is normally small, and in the center of the flow the isopycnals are essentially parallel to the bottom, so that the first order cross-stream balance in the center of the flow reduces to Eq. 2.

The downstream momentum balance for the mean flow is approximately between friction and the downslope component of buoyancy (e.g., Turner, 1973; Bo Pedersen, 1980);

$$V = (g'hs_y/C_f)^{1/2} \tag{3}$$

where C_f is a dimensionless parameter characterizing the bottom friction ($2 \times 10^{-3} < C_f < 3 \times 10^{-2}$). The along-stream slope (s_y) is about 0.01 inside the sill. This expression then gives 15 cm $s^{-1} < V < 60$ cm s^{-1}. These values also fall into the observed range of current speeds recorded by the lower current meters.

The speed of a density current surge on a sloping bottom is given by;

$$V_o = 0.75(g'h_o)^{1/2}, \tag{4}$$

where h_o is the thickness of the head (Turner, 1973). Using 25–40 m for h_o (based on the thermistor chain results in Figs. 8 and 9), and the value for g' stated above, gives an expected speed of 17–21 cm s^{-1}. The inferred propagation speeds of the cold temperature fronts were higher, between 35–70 cm s^{-1}. Account must be taken, however, of the advection of the fronts by the mean flow. The mean flow at the lower current meters was about 15 cm s^{-1}, so that adjusted propagation speeds of the fronts do fall roughly within the theoretical estimates. Whether the cold fronts really represent surge-type density currents, however, or simply long-wave perturbations to the mean flow, is unclear from our data. The long wave speed is roughly $\sqrt{g'h}$, which would give values similar to those above. Furthermore, the leading edge of a density surge is expected to have a 60° slope relative to the bottom. Even given the limitations of the thermistor chain 20-min sampling interval, the data in Figure 9 and the speed estimates do not indicate frontal slopes anywhere near this steep. This argues in favor of the long wave interpretation.

It seems reasonable to suggest that the inflow takes the form of a bottom gravity current in approximate geostrophic balance in the mean. The inflow exhibits properties similar to those observed in deep ocean gravity currents. The time variations associated with cold temperature fronts are either in the form of surges or long-wave perturbations to the mean flow, more likely the latter. The variability associated with these fronts is mainly at the diurnal period, suggesting a direct relationship with the tide. Longer period variability is also present (the 2.6-d oscillation). These sources of variability are discussed below.

b. Tidal forcing. There is a strong modulation of the overflow by both the diurnal and semidiurnal tide. This is evident both in the power spectra (Fig. 11) and the velocity

time series (Fig. 6c). The amplitude of the tidal modulation also displays a clear spring-neap cycle (Fig. 6c). The spring-neap cycle is also evident in the high-passed temperature data (Fig. 6d). This spring-neap modulation of the temperature fluctuations will affect the measurement of the heat flux associated with the inflow, a topic beyond the scope of this paper.

Estimates of the phase spectra suggest that tidal forcing at the semi-diurnal period is essentially barotropic. At the diurnal period, however, the phase spectra indicate baroclinic motion with a vertical wavelength of 270–450 m, which is 2–3 times the water depth at M1. At M1, the direction of phase propagation is upward. At M2, phase propagates downward. A peak in the current shear is also observed at the diurnal period at moorings M1 and M2.

Assuming linear theory for internal wave propagation in a channel of uniform buoyancy frequency (N) and total depth H, the predicted vertical wavelength (λ_v) for the first mode, in non-rotating dynamics, is $\lambda_v = 2H$ (Gill, 1982), with a corresponding phase velocity of $c_{int} = 2H/T \sin \beta$. Here T is the wave period and $\sin \beta = \sigma/N$, where β is the angle the group velocity vector relative to the horizontal, and σ is the angular frequency of the waves.

We may apply this simple theory to Fortune Bay. At the sill, where we might expect the internal motion to be generated, $H = 120$ m and hence λ_v will be about 240 m. This value is smaller than that estimated from the velocity cross spectra, but is consistent with the value found from the phase difference in temperature between the two current meters on M1. Considering the simple nature of approximating the stratification to a linear profile and the errors in estimating the phase differences using a short data set, the agreement is not bad. CTD casts close to the mooring array indicate that the mean buoyancy frequency is about $3–4 \times 10^{-3}$ s^{-1}, so that $\beta = 1–1.3°$. The phase measurements suggest downward energy propagation at the sill. Over a horizontal distance of 10 km, the separation between moorings 1 and 2, this would imply a vertical propagation of O(150–200 m). However, the depth increases by only 80 m between M1 and M2 (Table 1). This implies that reflection off the bottom would occur between the two mooring locations, and could explain the change from the downward direction of energy propagation at M1 to upward propagation at M2.

There are difficulties with the above treatment of the diurnal signals. The corresponding frequency is less than f, so vertically propagating waves with diurnal period would necessarily be evanescent. There is another possibility, and that is that the diurnal baroclinic signals are Kelvin waves or topographic waves, propagating into the bay with shallow water to the right. Such waves are not limited to frequencies greater than f, and can therefore carry information away from the sill into the main basin. Such waves could be responsible for the fronts discussed in the previous section. This is the interpretation which we favor. The downstream change in the vertical phase difference then requires a different interpretation. The effects of

friction on the vertical phase distribution should be included, as the lower current meter is well within the bottom Ekman layer.

c. Basin response. A distinct oscillation with period 2–3 d was observed in most velocity and temperature time series (Figs. 6 and 7). The rotary spectra also show a peak in the 0.2–0.5 cpd frequency band. This peak is centered at 2.6 d. The cross spectra indicate a high degree of coherence for this motion between individual moorings. The oscillation in current takes the form of an initial maximum pulse followed by a moderate decay in amplitude. The initiation of the oscillation appears correlated with the time of maximum inflow. Phase measurements between lower current meter pairs show that propagation at this period is from M1 to M3 and M4 (away from the sill) with an inferred phase speed of $O(55–70 \text{ cm s}^{-1})$. Between M2 and M1 the phase propagation is toward the sill with a speed of $O(15–20 \text{ cm s}^{-1})$. These directions of phase propagation suggest a motion propagating around the bay.

The difference in the estimated phase speeds for the two propagation directions might be accounted for by assuming an interaction between the mean flow and the wave propagating around the bay, producing a Doppler shift in the phase measurements. The mean flow into the bay was 15 cm s^{-1}. Adding or subtracting this velocity to the estimated lower level phase velocities gives adjusted phase velocities of 30–35 cm s^{-1} between M2 and M1 and 35–45 cm s^{-1} between M1 and M3/M4. These values are consistent, therefore, with the idea of a wave propagating around the bay with a phase speed of $O(30–35 \text{ cm s}^{-1})$.

Estimates of the first baroclinic mode wave speed (c_1) have been made from the CTD density profiles. Values of 35 cm $s^{-1} < c_1 < 50$ cm s^{-1} were found, with larger values found farther from the sill region in deeper water (where current measurements were not made). These values for baroclinic wave propagation are consistent with the adjusted wave speeds estimated from the phase measurements. We might assume a simple form for the spin down time of the motion due to friction, for example $\tau = H/(2C_dV_{av})$ (Gill, 1982). Here H is the depth of the water column, C_d a drag coefficient (3×10^{-3}) and V_{av} a mean current speed. Taking $H = 350$ m and $V_{av} = 15$ cm s^{-1}, gives $\tau = 4.5$ d. This is roughly consistent with the observations (Figs. 5 and 6).

Consider an internal seiche due to Kelvin wave propagation around the bay. The period T of such motions can be roughly estimated from $T = 2(D + L)/c$, where $D + L$ is the sum of the bay's length and width and c the phase velocity. Assuming a range of values 35 cm $s^{-1} < c < 50$ cm s^{-1} and $D + L = 140$ km, gives values of T in the range 6–9 d. This is longer than the period observed for the dominant oscillation in the time series (Fig. 6 and 7). It is conceivable that the 6–9 d estimate could be reduced by a factor of 2 or so, by including the possible effects of long-wave reflection from the plateau region (Fig. 1).

There remains the possibility of bottom-trapped waves within the bay. Such waves

have been investigated by Rhines (1970), who considered a rotating, stratified channel of width L and cross channel slope α. Waves may occur for frequencies $\omega < N \sin \alpha$, where N is the buoyancy frequency and propagate with shallow water to the right. The low frequency limit is $\alpha N/f < 1$. For Fortune Bay $\alpha = 0.01$, $N = 3 \times 10^{-3}$ s^{-1} so that $\alpha N/f = 0.3$. The essential parameters in the analysis are $\delta = \alpha L/H$, where H is the mean depth, and $B = NH/fL$. L is taken to be 10 km.

The solution for the non-dimensional pressure (P) for this limit is,

$$P = e^{ily} \sinh k_n x \cosh \mu z \tag{5}$$

where $\mu^2 = B^2(l^2 + k_n^2)$, $k_n = \pi, 2\pi$, etc. The x and y axes are in the cross- and along-channel directions, as previously defined, and are non-dimensionalized by L. The vertical coordinate z is 0 at the sea surface, positive upward, and is non-dimensionalized by H, and l and k_n are non-dimensional wavenumbers. For $\mu \geq 1$, the dimensional dispersion relation is found to be,

$$\omega = f\delta Bl/(l^2 + k_n^2)^{1/2} = \alpha N \sin \phi \tag{6}$$

where ϕ is the angle of the wave vector with respect to the x axis.

For Fortune Bay $B = 0.3$ so $\mu \geq 1$ for any choice of l, and the limit applies. For $\alpha = 0.01$ and $N = 3 \times 10^{-3}$ s^{-1} and taking $\phi = 90°$, then $\omega = 3 \times 10^{-5}$ s^{-1}, giving the period $T = 2.4$ d. This is the lower bound on T. For $\phi = 45°$, $T = 3.4$ d. This range of T agrees well with the observed periods of low-frequency variability in the bay (Figs. 6, 7 and 11). Note as well that since $\mu \geq 1$, these waves are bottom-intensified. In dimensional form, the vertical trapping scale (H_n) is;

$$H_n = f/N(l'^2 + k_n'^2)^{1/2} \tag{7}$$

where the wavenumbers ($l' + k_n'$) are now dimensional. For a 2.6 d wave, and using the dispersion relation, it is found that $l = 2.6\, k_n$. The trapping scale for $n = 1$ is then $H_1 = 40$ m, which is much less than the water depth.

The possibility that low-frequency variability in the dense bottom current might arise from coupling with bottom-trapped waves is appealing on physical grounds. It would not be surprising if a bottom-intensified flow were strongly coupled to bottom-intensified waves. The mechanism which generates such waves in Fortune Bay is probably related to the variability in the exchange at the sill, which itself is forced by the wind and tides. We again point out the pronounced oscillation in the wind with 3-d period (Fig. 10). The phase velocity of the free wave is only $c_1 = \omega/l = 3.5$ cm s^{-1}, however. This, and the 2.6-d period, yields a wavelength $\lambda_y = 7.9$ km. Such waves would require $O(100$ d) to propagate around the basin, which seems so long that a basin mode is unlikely. These waves are much shorter than the basin length (120 km), and shorter even than the M1–M2 separation (10 km). Figure 14 shows phase velocities inferred from the lag in the along-stream velocity at the 2.6 d period, between M1 and M2. The velocities were calculated, however, assuming that the

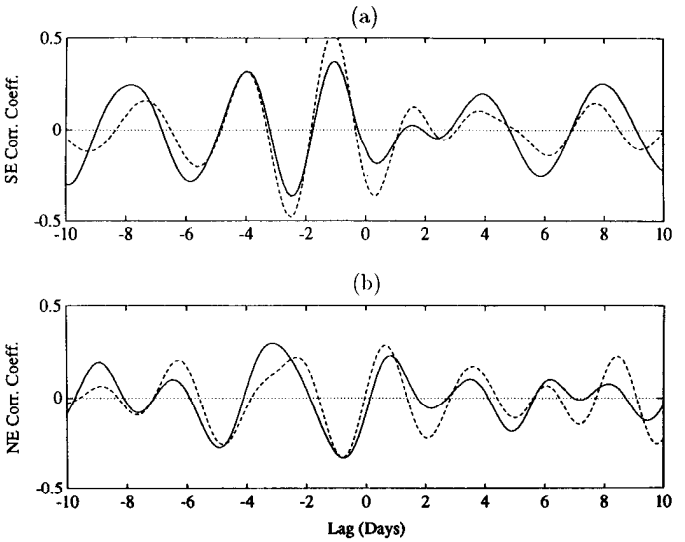

Figure 16. Cross-correlation functions between wind and the along-bay (v) current at M1, in the 2–5 d band. Solid lines represent lower current meter, dashed lines upper. (a) SE wind; (b) NE wind.

along-stream wavelength (λ_y) was much greater than the 10 km separation of the moorings, as for a seiche. Alternatively, if λ_y is less than 10 km, and assuming that the y-separation of the current meters is $\lambda_y + \Delta_y$, then the phase differences imply that $\lambda_y = 8.8$ km. This agrees remarkably well with the theoretical estimate, considering the rather complicated bathymetry of the basin in comparison to the simple channel geometry of the model.

d. Wind forcing. Figure 16 shows the lagged cross-correlation functions between the wind and the along-bay (v) component of the current at mooring M1, in the 2–5 d band. At the sill mooring, inflow is positively correlated with the SE wind component at both upper and lower levels, at a lag of about −1 d. (Note the increase in the peak correlation for the upper meter compared to Figure 10c.) In contrast, the inflow is negatively correlated with the NE wind component at both levels, the peak correlation also occurring at about −1 d. These results support the argument made earlier, on the basis of the low-passed signals, that the dense overflow into the bay is correlated with the wind blowing "out of the bay" in both the SE and SW directions, with the SE wind having the greatest effect (on the basis of the relatively higher peak correlations for this component). Note also the approximate 3-d periodicity in the SE wind correlation functions.

These results suggest that the 2–3 day oscillation in the currents may be wind-forced, at least partially. There are two possibilities. One is that the energy in the wind in the 2–3 day band couples directly to the currents by exciting a natural modal

response in the bay at this period. This would require that the periods of the long-wave seiche estimated above be reduced appropriately, perhaps by reflection from the plateau. The second possibility is that the wind modulates exchange at the sill, perhaps through upwelling/downwelling on the adjacent shelf. This could involve the generation of bottom-trapped waves, as discussed above. Distinguishing between the two candidate mechanisms, on the basis of the very different wavelengths associated with the seiche and bottom-trapped waves, would have required additional elements in our mooring array.

e. Baroclinic instability. Some of the variability observed in the time series may be the result of a baroclinic instability. The CTD casts indicate (Fig. 4) that at times the isopycnal slope does become as large as the cross-stream bottom slope, suggesting that instability may occur in the bottom flow.

In his study of the Denmark Strait overflow, Smith (1976) proposed an instability criterion based on the tilt of the isopycnals relative to the bottom slope. The instability criterion is that $S^{-1} > 1$, where $S^{-1} = fV/g's_x$, expresses the ratio of the Coriolis and buoyancy accelerations. Here s_x is the cross-stream bottom slope. For Fortune Bay $V = 20$ cm s^{-1} and $s_x = 0.01$ so that $S^{-1} = 0.1$. This would suggest that the overflow is not unstable. However, the criterion is valid for small Rossby Number, $\epsilon = V/fL_x$, where L_x is the channel width. For $L_x = 10$ km, $\epsilon = 0.2$ here, so that it is unclear that the non-linear terms may be neglected in this situation.

Swaters (1991) has analyzed the baroclinic instability of cold-core coupled density fronts on a sloping shelf. Swater's criterion for instability is that the average correlation between the perturbation cross shelf flow and the frontal height anomaly should be positive, i.e.

$$\int u_1' h' \, dy > 0, \tag{8}$$

where u'_1 is the across-shelf perturbation velocity above the density current and h' the frontal height anomaly. The integral is evaluated across the width of the density current. Values of $\langle u'_1 h' \rangle$ have been evaluated at moorings 1, 2 and 4 over the 70-d observation period. Mean values of 0.13, 0.07 and 0.014 were found respectively. The positive values of $\langle u'_1 h' \rangle$ at both M2 and M4 suggest that the integral would be positive when evaluated across the density current at the mooring line position. This suggests that the bottom flow may become unstable using this criterion. The stability characteristics are determined by a scale quantity, $\nu = h/s_y l_x$. This parameter measures the ratio between the destabilizing baroclinic vortex stretching/compression and the stabilizing beta-plane effect of the across-stream bottom slope. Taking $l_x = 2$ km (the Rossby radius) as a cross-stream lengthscale, $h = 50$ m, and $s_y = 0.01$ gives $\nu = 2.5$. For small ν any instability that might develop will have a long down-stream wavelength and growth time of $O(10$ d). (For $\nu = 2$, Swaters obtained a growth time of 8 d.) This timescale is longer than the dominant variability timescale

observed in the data. Note the growth time increases as l_x increases. The value of 2 km is probably a minimum for l_x, so that growth times could actually be longer.

6. Conclusions

The overflow of cold, dense Labrador water into a silled embayment has been observed for a 70-d period. The scale of the bay is large enough that the Coriolis force plays a role in the overflow dynamics and the inflow takes the form of a density current in approximate geostrophic balance. The inflow is modulated at the semi diurnal, diurnal and spring-neap periods, as well as by the local wind forcing. A distinct oscillation of period O(2.5–3 d) is observed in the time series. It appears likely that this represents a natural frequency of the system, associated with a bottom-trapped baroclinic wave mode, which may be resonantly excited by the wind. It is suggested that the coupling between the wind forcing and the wave mode occurs at the mouth of the bay, where divergence in the wind-induced transport in the upper layer may produce variations in the overflow which then radiate away from the sill into the bay as bottom trapped topographic waves.

The dense overflow into Fortune Bay persisted throughout the 70-d measurement period. It appears to be a seasonal feature, recurring from year-to-year (Hay and DeYoung, 1989). Because of the large dimensions of the bay in relation to the internal deformation radius, the overflow exhibits analogous behavior to the dense overflows in the deep ocean. This behavior, together with its persistence and annual recurrence, make the Fortune Bay overflow an interesting case study in the dynamics of overflows affected by rotation. The present study indicates, however, that the extent to which the Fortune Bay overflow can be used as a surrogate for its deep ocean counterparts may be limited in part by the spectral overlap between the forcing and the basin response. The resulting coupling between the forcing and the basin modes is a complication not present in the same form for larger basins. Nevertheless, the suggestion made here that the variability in the Fortune Bay overflow may be partly controlled by coupling to the overlying fluid via bottom-trapped waves would seem to have application to deep ocean overflows. Nof (1984) showed, for a two-layer model of a rotating dense bottom current, propagating shocks would form as a result of Kelvin waves generated by temporal variability in the source discharge. By allowing for continuous density stratification in the fluid above the density current, we suggest that bottom-trapped waves may provide an additional mechanism for propagating information downstream in modulated rotating dense bottom currents.

Acknowledgments. The authors thank Jack Foley for his indispensable help in collecting the data, and the Masters and crews of the RV *Dawson* and RV *Shamook* for their expertise and co-operation during the data collection. We also thank Mr. Alan Goulding, who developed the computer movie from which Figure 5 was obtained.

REFERENCES

Bo Pederson, F. 1980. A monograph on turbulent entrainment and friction in two-layer stratified flow. Institute of Hydrodynamics and Hydraulic Engineering, Technical University of Denmark, 397 pp.

De Young, B. and A. E. Hay. 1987. Density current flow into Fortune Bay, Newfoundland. J. Phys. Oceanogr., *17,* 1066–1070.

Dickson, R. R., E. M. Gmittrowicz and A. J. Watson. 1990. Deep water renewal in the northern North Atlantic. Nature, *344,* 848–850.

Farmer, D. M. and H. J. Freeland. 1983. The physical oceanography of fjords. Progr in Oceanogr, *12,* 147–220.

Gade, H. G. and A. Edwards. 1980. Deep water renewal in fjords, *in* Fjord Oceanography, H. J. Freeland, D. M. Farmer and C. D. Levings, eds., Plenum Press, New York, 453–489.

Geyer, W. R. and G. A. Cannon. 1982. Sill processes related to deep water renewal in a fjord. J. Geophys. Res., *87,* 7985–7996.

Gill, A. E. 1982. Atmosphere-Ocean Dynamics, Academic Press, 662 pp.

Hay, A. E. and B. De Young. 1989. An oceanographic flip-flop: deep water exchange in Fortune Bay, Newfoundland. J. Geophys. Res., *94,* 843–853.

Nof, D. 1984. Shock waves in currents and outflows. J. Phys. Oceanogr., *14,* 1683–1702.

Price, J. F., M. O. Baringer, R. G. Lueck, G. C. Johnson, I. Ambar, G. Parrilla, A. Cantos, M. A. Kennelly and T. Sanford. 1993. Mediterranean outflow mixing and dynamics. Science, *259,* 1277–1282.

Rhines, P. 1970. Edge-, bottom-, and Rossby waves in a rotating stratified fluid. Geophys. Fluid Dyn. *1,* 273–302.

Saunders, P. M. 1990. Cold outflow from the Faroe Bank channel. J. Phys. Oceanogr., *20,* 29–43.

Smith, P. C. 1975. A streamtube model for bottom boundary currents in the ocean. Deep-Sea Res., *22,* 853–873.

—— 1976. Baroclinic instability in the Denmark Strait overflow. J. Phys. Oceanogr., *6,* 355–371.

Stanton, B. R. 1983. Low frequency variability of the Mediterranean Outflow west of Gibraltar. Deep-Sea Res., *30,* 743–761.

Swaters, G. E. 1991. On the baroclinic instability of cold-core coupled density fronts on a sloping continental shelf. J Fluid Mech., *224,* 361–382.

Turner, J. S. 1973. Buoyancy Effects in Fluids, Cambridge University Press, 368 pp.

Zenk, W. and L. Armi. 1990. The complex spreading pattern of Mediterranean Water off the Portuguese continental slope. Deep-Sea Res., *37,* 1805–1823.

Received: *29 May, 1993;* revised: *25 January, 1994.*